

## Entropic forces in dilute colloidal systems

R. Castañeda-Priego

*Instituto de Física, Universidad de Guanajuato, Lomas del Bosque 103, Col. Lomas del Campestre, 37150 León, Guanajuato, Mexico*

A. Rodríguez-López and J. M. Méndez-Alcaraz

*Departamento de Física, Cinvestav, Av. IPN 2508, Col. San Pedro Zacatenco, 07360 México, Distrito Federal, Mexico*

(Received 10 March 2006; published 25 May 2006)

Depletion forces can be accounted for by a contraction of the description in the framework of the integral equations theory of simple liquids. This approach includes, in a natural way, the effects of the concentration on the depletion forces, as well as energetic contributions. In this paper we systematically study this approach in a large variety of dilute colloidal systems composed of spherical and nonspherical hard particles, in two and in three dimensions, in the bulk and in front of a hard wall with a relief pattern. We show by this way the form in which concentration and geometry determine the entropic interaction between colloidal particles. The accuracy of our results is corroborated by comparison with computer simulations.

DOI: [10.1103/PhysRevE.73.051404](https://doi.org/10.1103/PhysRevE.73.051404)

PACS number(s): 82.70.-y, 61.20.Gy

### I. INTRODUCTION

Complex fluids are composed of a large amount of particles of many different species. For example, a clean aqueous suspension of polystyrene spheres contains, obviously, the polystyrene spheres and the water molecules, but also ions dissociated from the surface of the spheres, called counterions, and at least two different species of salt ions. The size of the first ones ranges from about some tens of nanometers, up to several microns. The other particles are of subnanometer dimensions. When looking at this suspension by means of light scattering, for example, only the big spheres seem to be present in the system, since they are the only ones able to affect the photons of wavelengths of the order of micrometers. Therefore, in this example the experimental access to the system is limited, and we can only observe a part of it. The physics of this part, however, is determined by all the existing particles, observed or not. Regardless of the kind of condensed matter system that we might be able to imagine, and of the experimental method that we might propose in order to look inside it, the conclusion is always the same: We can observe only a part of the system, but the physics of this part is also determined by the rest. Physicists deal with the restricted nature of the experimental observations by developing contracted pictures, or effective theories, containing parameters related to the unobserved variables. The basic concept behind this kind of approach is the effective pair interaction potential between the observed particles. Depletion forces are a particular case of this kind of interaction, which describe the phase of a great variety of colloidal and polymeric systems with an important excluded volume contribution to the free energy.

The term depletion forces originally refers to the attraction between two colloidal particles arising when macromolecules are put into the suspension [1,2]. This attraction results from the expulsion of added macromolecules from the gap between two approaching particles, giving rise to an imbalance between the osmotic pressures inside the gap and outside it and, therefore, to a decrease of the free energy of the system when the particles come together. This phenomenon has been successfully studied in the usual case that the system can be modeled as a binary mixture of hard spheres,

as in the case of uncharged globular macromolecules and spherical colloidal particles, by means of perturbations theory [3,4], density functional theory [5–7], and integral equations theory [8]. Moreover, some attempts to account for polymer nonideality beyond the hard spheres model have also been reported, using extensions of the theoretical frameworks mentioned above [8–11], as well as self-consistent mean field calculations [12]. Indeed, depletion forces can be strongly affected if van der Waals or coulombic interactions are present in the system.

With regard to the relative merits of each approach, it can be said that perturbations theory straightforwardly allows for the incorporation of some geometrical effects on the depletion forces, as in the case of a mixture of spherical and nonspherical colloidal particles [13,14], but makes it very difficult to include concentration effects and energetic contributions in the theoretical scheme [4]. The approaches based on the density functional theory (DFT) incorporate otherwise, additionally to some geometrical effects, as in the case of a colloidal mixture in front of a curved hard wall [15,16], concentration effects in a natural way. However, the energetic contributions to the depletion forces are only very hard to capture. Finally, the approach based on the integral equations theory (IET) captures both concentration effects and energetic contributions in a natural way, and, as we show in this work and in a previous paper, also the effects of the geometry of the components of the colloidal system [17]. In addition, IET seems to work better than DFT for systems in even dimensions [18,19]. The method based on the DFT works better in extreme situations, as in the case of very large differences in the size of the colloidal particles, but the approach based on the IET is far easier to implement, both schemes providing an excellent quantitative description of the depletion forces, when they are compared with computer simulations. Actually, the distinction we make between density functional theory and integral equations theory is quite artificial. In fact, IET can be obtained from DFT [20]. Nevertheless, once the equations of IET are obtained from DFT, the methods to work with them differ from the methods of DFT to such an extent that both are very often identified in the literature as different routes.

The integral equations theory represents a natural starting point for the implementation of the contraction formalism from which the depletion forces are determined. The basic idea is that depletion forces are a special case of the more general effective interactions resulting from a contraction of the description of liquid mixtures. Therefore, if certain components of a mixture are not explicitly considered, their influence on the structure of the remaining particles has to be included in the effective interaction potential between the latter ones. This is obtained by demanding the spatial distribution of the “observed” particles to be the same as in the original mixture. Technically, this is done by rewriting the Ornstein-Zernike equation for the original mixture as an effective Ornstein-Zernike equation for the remaining particles, and connecting it with the effective interaction potential by means of an appropriate closure relation. This idea was first implemented in order to calculate the interaction between two charged macroions immersed in a bath of small counterions and salt ions [21], as well as in further approaches to the same problem [22,23]. We consider here the case of large hard spheres immersed in a bath of smaller spherical and nonspherical hard particles in order to describe depletion forces of only entropic nature. In this paper we systematically study a large variety of dilute colloidal systems composed of spherical and nonspherical particles, in two and in three dimensions, in the bulk and in front of a hard wall with a relief pattern. We show by this way the form in which concentration and geometry determine the entropic interaction between colloidal particles, leading to surprising results. For instance, the design of surfaces of entropic potential.

After a brief introduction, we summarize in Sec. II the integral equations theory of liquid mixtures. Then, the contraction of the description procedure and its meaning are explained in Sec. III. Here, some computer simulation results for two-dimensional binary mixtures of hard disks are shown in order to clarify some of the involved ideas. In Sec. IV the general formulation of depletion forces in multicomponent systems is presented, and the resulting equations are explicitly written for dilute systems. In Sec. V the particular cases of two- and three-dimensional binary and ternary mixtures are discussed. Section VI deals with colloidal mixtures in front of a flat, or concave, or convex hard wall. The results obtained in Sec. VI are carefully worked up in Sec. VII to a method of entropic engineering, which allows the design of surfaces of entropic potential. The effects of the geometry of the components of the system are addressed in Sec. VIII, where three-dimensional binary mixtures of hard spheres and hard spherocylinders are studied. Section IX deals with concentration effects and energetic contributions, as far as it is possible to obtain information about from the dilute limit in our equations. Finally, the paper ends with a section of conclusions.

## II. INTEGRAL EQUATIONS THEORY

In an homogeneous colloidal mixture of  $p$  spherical species, the total correlation  $h_{ij}(r)$  between a particle of species  $i$  and a particle of species  $j$ , separated by the distance  $r$ , can

be expressed in a logical, almost graphical form by the expansion

$$\begin{aligned} h_{ij}(r) = & c_{ij}(r) + \sum_{k=1}^p n_k \int_V c_{ik}(r') c_{kj}(|\mathbf{r} - \mathbf{r}'|) d\mathbf{r}' \\ & + \sum_{k,l=1}^p n_k n_l \int_V \int_V c_{ik}(r') c_{kl}(r'') c_{lj}(|\mathbf{r} - \mathbf{r}' - \mathbf{r}''|) d\mathbf{r}' d\mathbf{r}'' \\ & + \dots, \end{aligned} \quad (1)$$

where the function  $c_{ij}(r)$  represents the direct correlation between particles  $i$  and  $j$ , defined in such a way that  $h_{ij}(r)$  includes all possible correlations involving all the  $N = \sum_{i=1}^p N_i$  particles in the volume  $V$ ;  $N_i$  is the number of particles of species  $i$  and  $n_i = N_i/V$  its bulk number density. The second term of the right hand side of Eq. (1) represents all links between two particles mediated by a third one. The third term of the right hand side represents all links between two particles mediated by two other particles, and so forth. In highly dilute systems, the direct correlation function reduces to the pair interaction potential  $u_{ij}(r)$  between the particles, so far they do not overlap, scaled with the thermal energy;  $c_{ij}(r) = -u_{ij}(r)/k_B T$  [24]. The minus sign guarantees that the total correlation function at short distances becomes negative (positive) for repulsive (attractive) interactions.

Equation (1) is a geometrical series and can therefore be rewritten as the well known Ornstein-Zernike equation (OZ) [24],

$$h_{ij}(r) = c_{ij}(r) + \sum_{k=1}^p n_k \int_V c_{ik}(r') h_{kj}(|\mathbf{r} - \mathbf{r}'|) d\mathbf{r}', \quad (2)$$

which needs a closure relation linking the structure functions  $h_{ij}(r)$  and  $c_{ij}(r)$  with the pair interaction potential  $u_{ij}(r)$  for its solution. This closure relation has the following general form [24]

$$c_{ij}(r) = -\beta u_{ij}(r) + h_{ij}(r) - \ln[1 + h_{ij}(r)] + b_{ij}(r), \quad (3)$$

where  $\beta = 1/k_B T$  and  $b_{ij}(r)$  is a structure function known as bridge function. Further approximations for  $b_{ij}(r)$  are necessary in order to close the scheme.

One of the most successful closure relations is an empirical one proposed by Rogers and Young (RY) [25], which has the form

$$c_{ij}(r) = \exp[-\beta u_{ij}(r)] \left[ 1 + \frac{\exp[\gamma_{ij}(r) f_{ij}(r)] - 1}{f_{ij}(r)} \right] - \gamma_{ij}(r) - 1. \quad (4)$$

Here,  $\gamma_{ij}(r) = h_{ij}(r) - c_{ij}(r)$  is the indirect correlation function and  $f_{ij}(r) = 1 - \exp(-\alpha_{ij} r)$  is the mixing function. The mixing parameter  $\alpha_{ij}$  is obtained by demanding thermodynamic consistency of the solution of OZ. This can be illustrated by remembering the contribution of Biben and Hansen [26,27], where they studied asymmetric binary mixtures ( $p=2$ ) of hard spheres by means of OZ+RY. The mixing parameter was obtained in their work from the assumption that it scales with the contact distance between particles,  $\alpha_{ij} = \alpha/\sigma_{ij}$ , and by fixing  $\alpha$  by demanding the same value of the isothermal

compressibility as calculated from the compressibility equation of state [24],

$$\left(\frac{\partial[\beta P]}{\partial n}\right)_T = 1 - n \sum_{i,j=1}^2 x_i x_j \tilde{c}_{ij}(0), \quad (5)$$

and from the differentiation of the virial equation of state [24],

$$\frac{\beta P}{n} = 1 + \frac{2\pi n}{3} \sum_{i,j=1}^2 x_i x_j \sigma_{ij}^3 g_{ij}(\sigma_{ij}^+). \quad (6)$$

Here,  $\sigma_{ij} = (\sigma_i + \sigma_j)/2$  is the contact distance between particles,  $\sigma_i$  is the diameter of the particles of species  $i$ ,  $n = \sum_{i=1}^p n_i$  is the total bulk density,  $x_i = n_i/n = N_i/N$  is the molar fraction of species  $i$ ,  $g_{ij}(r) = h_{ij}(r) + 1$  is the partial radial distribution function,  $P$  is the osmotic pressure in the system, and  $\tilde{c}_{ij}(0)$  denotes the Fourier transform  $\tilde{c}_{ij}(q)$  of  $c_{ij}(r)$  evaluated at  $q=0$ . Since the closure relations are approximations, their use in calculating thermodynamic properties will lead, in general, to different results, when the properties are determined by using different routes. Instead, by implementing RY the value of  $\alpha$  can be fixed by demanding the restoration of thermodynamic consistency, at least partially, as seen above.

Biben and Hansen were mainly interested in the behavior of the long wavelength limit ( $q \rightarrow 0$ ) of the concentration-concentration structure factor  $S_{cc}(q)$ , given by [28]

$$S_{cc}(q) = x_2^2 S_{11} - 2x_1 x_2 S_{12}(q) + x_1^2 S_{22}(q), \quad (7)$$

since its divergence signals the end of thermodynamic stability with respect to phase separation, as can be seen from the equation of state [28]

$$S_{cc}(0) = \frac{Nk_B T}{(\partial^2 G / \partial x_1^2)_{N,P,T}}. \quad (8)$$

Here,  $S_{ij}(q) = x_i \delta_{ij} + n x_i x_j \tilde{h}_{ij}(q)$  is the partial structure factor and  $G$  the Gibbs free energy of the system. By using OZ in order to write  $S_{ij}(q)$  in terms of  $\tilde{c}_{ij}(q)$ , Eq. (7), together with the condition  $S_{cc}(0) \rightarrow \infty$ , leads to the expression

$$n_1 \tilde{c}_{11}(0) + \frac{n_1 n_2 \tilde{c}_{12}^2(0)}{1 - n_2 \tilde{c}_{22}(0)} = 1 \quad (9)$$

for the spinodal curve characterizing the phase separation. It means that the particles in the system demix when Eq. (9) is fulfilled. Biben and Hansen found that it may occur for size ratios  $\sigma_1/\sigma_2 \geq 5$ . Indeed, this prediction has been corroborated by several authors, by means of experiments [29–34] and of computer simulations [35–37]. They observed that the segregated big particles condense in a phase whose density is larger than the density of the same species in the homogeneous system. This result will help us to understand the meaning of the contraction of the description explained in the next section. It is widely accepted that binary hard spheres in three dimensions exhibit a gas-liquid separation for a certain range of size ratios, but all of which seems to be preempted by the freezing transition, i.e., the gas-liquid transition is metastable with respect to freezing [38].

### III. CONTRACTION OF THE DESCRIPTION

As seen in the previous section, the structure of an homogeneous colloidal mixture of  $p$  spherical species is given by the OZ equation [24]

$$\tilde{h}_{ij}(q) = \tilde{c}_{ij}(q) + \sum_{k=1}^p n_k \tilde{c}_{ik}(q) \tilde{h}_{kj}(q), \quad (10)$$

written here in the Fourier space. This equation owns a very important, but not much exploited property: It does not change its form when only a part of the system can be observed, i.e., its form is invariant under contractions of the description. Let us suppose, without loss of generality, that we can only observe the particles of species 1 in the mixture of  $p$  components. In a light scattering experiment, for example, this condition can be imposed by the wavelength of the light, if it is comparable to  $\sigma_1$  but very much larger than the diameters of the other components. The other species are there, but we suppose to ignore that fact. Therefore, we describe the structure of the observed particles by means of the monodisperse OZ equation

$$\tilde{h}_{11}(q) = \tilde{c}_{11}^{eff}(q) + n_1 \tilde{c}_{11}^{eff}(q) \tilde{h}_{11}(q). \quad (11)$$

Since  $\tilde{h}_{11}(q)$  is a quantity which can be measured, it has to be the same in both Eqs. (10) and (11), then the particles have the same structure regardless of our ability to distinguish the different kinds of components. The other species not longer appear as separated species in Eq. (11). Instead, their effects on the structure of component 1 are included in  $\tilde{c}_{11}^{eff}(q)$ . This fact is denoted by the superindex *eff*. The new effective direct correlation function can be obtained in terms of the direct correlation functions of the original mixture by rewriting Eq. (10) in the monodisperse form (11), i.e., exploiting the invariance of the form of the OZ equation under contractions of the description. This leads to [8]

$$\begin{aligned} \tilde{c}_{11}^{eff}(q) &= \tilde{c}_{11}(q) + \sum_{i \neq 1}^p \frac{\tilde{c}_{1i}(q) n_i \tilde{c}_{i1}(q)}{[1 - n_i \tilde{c}_{ii}(q)]} \\ &+ \sum_{i \neq 1}^p \sum_{j \neq 1, i}^p \frac{\tilde{c}_{1i}(q) n_i \tilde{c}_{ij}(q) n_j \tilde{c}_{j1}(q)}{[1 - n_i \tilde{c}_{ii}(q)][1 - n_j \tilde{c}_{jj}(q)]} + \dots \end{aligned} \quad (12)$$

In addition, the effective interaction potential  $u_{11}^{eff}(r)$  can be obtained from Eqs. (11) and (12) by using a closure relation of the general form [24]

$$c_{11}^{eff}(r) = -\beta u_{11}^{eff}(r) + h_{11}(r) - \ln[1 + h_{11}(r)] + b_{11}^{eff}(r), \quad (13)$$

as we will see in the next section. Equation (12) can be written in closed form by using matrix notation [11,22]. Its present form, however, makes its application easier in the following sections, since it straightforwardly takes a very simple closed form in the case of binary and ternary mixtures.

Once the description is reduced, we can also calculate the thermodynamic properties of the system composed of only the observed species. The isothermal compressibility  $\chi_T$ , for example, is given by [24]

$$\chi_T^{-1} = 1 - n_1 \tilde{c}_{11}^{eff}(0). \quad (14)$$

The expression for the spinodal curve characterizing a phase transition between two phases of different densities can be obtained from Eqs. (12) and (14), together with the condition  $\chi_T \rightarrow \infty$ . For binary mixtures ( $p=2$ ) it leads to

$$n_1 \tilde{c}_{11}(0) + \frac{n_1 n_2 \tilde{c}_{12}^2(0)}{1 - n_2 \tilde{c}_{22}(0)} = 1, \quad (15)$$

which exactly agrees with Eq. (9) for the spinodal instability with respect to phase separation in the original binary mixture. When the condition (9) is fulfilled, the particles in the mixture segregate. Equation (15) tells us that this phenomenon looks like a gas-liquid phase transition when only the particles of species 1 are observed, which agrees with the experimental observations in asymmetric binary mixtures of hard spheres, as well as with computer simulation results for the same systems (this gas-liquid phase transition is, however, metastable with respect to freezing [38]). In general, the thermodynamic properties of the original mixture are not all captured by the reduced description. However, the properties depending only on the structure of the surviving species, which is invariant under contractions of the description, can still be obtained from the reduced system, as in the case of Eqs. (9) and (15).

In the original mixture the particles get the structure described by  $h_{ij}(r)$  due to their thermal agitation and to the interactions given by  $u_{ij}(r)$ ,  $i, j=1, \dots, p$ . In the case where we can only observe the particles of species 1, they get the same structure  $h_{11}(r)$  as in the original mixture, but due to the thermal agitation and to the effective interaction potential  $u_{11}^{eff}(r)$ . The latter can be obtained, at a molecular level, from the integration of the average forces calculated by fixing two particles of species 1, separated by the distance  $r$ , and by integrating the linear moment exchange between all the particles of the other species and the two fixed particles of species 1. We carried out this calculation in a two-dimensional binary mixture ( $p=2$ ) of hard disks by means of molecular dynamics simulations (MD), for the cases of infinite dilution of species 1 ( $n_1 \rightarrow 0$ ), size ratios  $\sigma_1/\sigma_2=5$  and 10, and concentrations  $\varphi_2=0.2$  and 0.4. Here,  $\varphi_i = \pi n_i \sigma_i^2 / 4$  is the two-dimensional filling fraction of species  $i$ . The computer simulations were performed in a quadratic simulation box with standard periodic boundary conditions, using the Verlet algorithm [39]. The number of particles used in this work for  $\sigma_1/\sigma_2=5$  was  $N_1=2$  and  $N_2=186$  (460) for  $\varphi_2=0.2$  (0.4). For  $\sigma_1/\sigma_2=10$  we used  $N_1=2$  and  $N_2=408$  (830) for  $\varphi_2=0.2$  (0.4). The length  $L$  of the simulation box was adjusted to give the prescribed density of the system according to the relation  $L^2 = N_2/n_2$ . At the beginning of the simulation, the two larger hard disks were placed at the center of the simulation box, separated by the distance  $r$ , remaining fixed in that position. The smaller hard disks were then placed randomly in the simulation box in a nonoverlapping configuration and allowed to move according to the Verlet algorithm, until equilibrium was reached. Further configurations were generated to calculate the average linear moment exchange. The same procedure was repeated for different values of  $r$  in

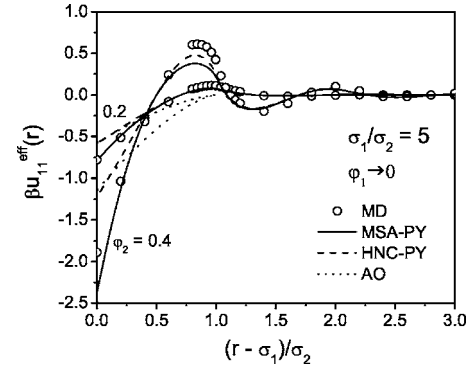


FIG. 1. The figure shows the depletion potential  $\beta u_{11}^{eff}(r)$  for two-dimensional binary mixtures of hard disks in the infinite dilute limit of particles of species 1,  $\varphi_1 \rightarrow 0$ , for the size ratio  $\sigma_1/\sigma_2=5$ , and filling fractions  $\varphi_2=0.2$  and 0.4 of the particles of species 2. The open symbols were obtained from molecular dynamics simulations. The full lines correspond to the results obtained from the MSA-PY approximation, the dashed lines to the results obtained from the HNC-PY approximation, and the dotted lines to the dilute limit in our equations.

order to get the average force in the whole range of significant separations. The effective interaction potentials results from the integration of the average force. The length  $L$  was always large enough for the smaller disks to get their bulk structure on the border of the simulation box. Therefore, the larger particles at the center of one cell do not feel the other particles of the same species in the other cells.

The effective interaction potentials calculated by MD are shown in Figs. 1 and 2 by the open symbols. The original binary mixtures are composed of hard disks of two different diameters. Their interactions are only of exclude volume type and, therefore, the free energy of the mixtures is only of entropic nature. If we are not able to observe the particles of species 2, although they are present in the system, which we

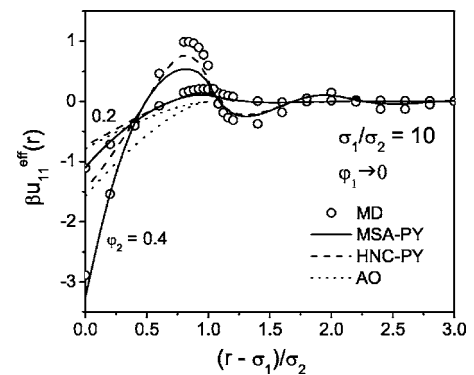


FIG. 2. The figure shows the depletion potential  $\beta u_{11}^{eff}(r)$  for two-dimensional binary mixtures of hard disks in the infinite dilute limit of particles of species 1,  $\varphi_1 \rightarrow 0$ , for the size ratio  $\sigma_1/\sigma_2=10$ , and filling fractions  $\varphi_2=0.2$  and 0.4 of the particles of species 2. The open symbols were obtained from molecular dynamics simulations. The full lines correspond to the results obtained from the MSA-PY approximation, the dashed lines to the results obtained from the HNC-PY approximation, and the dotted lines to the results obtained from the dilute limit in our equations.

suppose to ignore, we observe a monodisperse suspension composed of particles of species 1 interacting with the potential  $u_{11}^{eff}(r)$  shown in Figs. 1 and 2, which is long-ranged. Thus, the free energy of the effective monodisperse system contains a finite contribution from the excess energy. This constitutes an interesting result: One can go from an entropic system to an energetic system by ignoring a part of it. Alternatively, we can also say that the original binary mixture is an entropic picture of the monodisperse system, the latter in the sense that the particles of species 1 have the same structure in the entropic mixture as in the monodisperse suspension with interaction  $u_{11}^{eff}(r)$ . This assumption was corroborated by other authors [40], who performed computer simulations for three-dimensional binary mixtures of hard spheres, for either the entropic mixture and the contracted monodisperse suspension. The radial distribution function  $g_{11}(r)$  they found was the same in both cases. Although our simulations were done for the infinite dilute limit of the observed particles,  $n_1 \rightarrow 0$ , this does not affect the generality of our results. Indeed, the contraction of the description is a very general concept which can be applied even in the case that we can only see two of the suspended particles. The rest of them, of the same and of different species, determines the effective interaction potential between the two observed particles, as addressed in Ref. [41]. In that special case, when working with monodisperse systems,  $u_{11}^{eff}(r)$  and the potential of mean force  $w_{11}(r) = -\ln[1 + h_{11}(r)]$  are the same.

The attractive well at contact shown in Figs. 1 and 2 is due to the depletion effect arising from the expulsion of small particles from the gap between the two large particles. As expected from the Asakura-Oosawa approximation (AO) [1,2], its depth increases with  $\varphi_2$  and with  $\sigma_1/\sigma_2$ . Simultaneously, a potential barrier develops in front of the attractive well, and the interaction becomes more long-ranged, oscillating around zero at larger separations. This is due to the correlations between the contracted particles, which are not included in AO. We now develop a method able to capture such effects.

#### IV. ENTROPIC POTENTIALS

The effective interaction potential  $u_{11}^{eff}(r)$  is obtained from Eq. (13), where  $c_{11}^{eff}(r)$  is given by the inverse Fourier transform of Eq. (12), and  $b_{11}^{eff}(r)$  needs further approximations. If we take, for example,  $b_{11}^{eff}(r)=0$ , we get  $u_{11}^{eff}(r)$  from the hypernetted chain approximation (HNC) [24]:

$$\begin{aligned} \beta u_{11,HNC}^{eff}(r) &= +\infty \text{ for } r < \sigma_1 \\ &= -c_{11}^{eff}(r) + h_{11}(r) - \ln[1 + h_{11}(r)] \text{ for } r \geq \sigma_1. \end{aligned} \quad (16)$$

In the mean spherical approximation (MSA) [24] we get

$$\begin{aligned} \beta u_{11,MSA}^{eff}(r) &= +\infty \text{ for } r < \sigma_1 \\ &= -c_{11}^{eff}(r) \text{ for } r \geq \sigma_1. \end{aligned} \quad (17)$$

One more approximation must still be done in order to obtain the structure functions  $h_{ij}(r)$  and  $c_{ij}(r)$  of the original mix-

ture, so that we can evaluate  $c_{11}^{eff}(r)$ . Since the hard-core interaction between overlapping particles never changes, next we only try with the nonoverlapping part of the interaction potentials, i.e., with  $r \geq \sigma_1$ .

In the case of binary mixtures  $c_{11}^{eff}(r)$  becomes

$$c_{11}^{eff}(r) = c_{11}(r) + \mathcal{F}^{-1} \left\{ \frac{n_2 \tilde{c}_{12}^2(q)}{1 - n_2 \tilde{c}_{22}(q)} \right\}, \quad (18)$$

where the symbol  $\mathcal{F}^{-1}\{X\}$  denotes the inverse Fourier transform of  $X$ . If we take, for example, the Percus-Yevick approximation (PY) [24],

$$c_{ij}(r) = \exp[-\beta u_{ij}(r)] [\gamma_{ij}(r) + 1] - \gamma_{ij}(r) - 1, \quad (19)$$

for the binary mixtures of hard disks of the simulations shown in Figs. 1 and 2, we get the results shown in the same figures for  $\beta u_{11,HNC-PY}^{eff}(r)$  and  $\beta u_{11,MSA-PY}^{eff}(r)$ . In the notation  $u_{11,X-Y}^{eff}(r)$  the symbol  $X$  stands for the approximation used for  $b_{11}^{eff}(r)$  in Eq. (13), and the symbol  $Y$  for the approximation used in the calculation of the structure functions of the original mixture. The theoretical results and the MD data qualitatively agree in the whole range of significant separations. There are, however, appreciable quantitative differences in the depth of the attractive well in the contact region and in the height of the repulsive barrier in front of it. HNC-PY considerably underestimates the depth of the depletion well, and MSA-PY overestimates it a little. Both approximations, HNC-PY and MSA-PY, underestimate the height of the repulsive barrier. These differences, however, are rather similar to those normally observed when studying the structure of liquids [42]. Actually, the determination of the accuracy of the approximations done in the integral equations theory of liquids is often an empirical task. Therefore, we can speak only *a posteriori* about the accuracy of our approximations for  $u_{11}^{eff}(r)$ . This leads to some unexpected results. For example, if we take RY for  $h_{ij}(r)$  and  $c_{ij}(r)$ , and MSA for  $b_{11}^{eff}(r)$ , we get an effective interaction potential,  $u_{11,MSA-RY}^{eff}(r)$ , which is much more inaccurate than  $u_{11,MSA-PY}^{eff}(r)$ , although RY is a better approximation than PY for the structure of the original mixture (this result is not shown in the Figs. 1 and 2, but in Ref. [18]). The structure functions  $h_{ij}(r)$  and  $c_{ij}(r)$  of the original mixture were obtained in this paper from the numerical solution of Eq. (2) by means of a five parameters version of the Ng algorithm [43].

MSA-PY seems to be a very good approximation. This can be understood from Eqs. (3) and (13), which together lead to

$$\beta u_{11}^{eff}(r) = \beta u_{11}(r) + [c_{11}(r) - c_{11}^{eff}(r)] + [b_{11}^{eff}(r) - b_{11}(r)]. \quad (20)$$

This result means that  $\beta u_{11}^{eff}(r)$  is given by  $\beta u_{11}(r)$  plus the correlations terms  $c_{11}(r) - c_{11}^{eff}(r) + b_{11}^{eff}(r) - b_{11}(r)$ . If we neglect the difference between the bridge functions, not the bridge functions self, we get the expression

$$\beta u_{11}^{eff}(r) = \beta u_{11}(r) - \mathcal{F}^{-1} \left\{ \frac{n_2 \tilde{c}_{12}^2(q)}{1 - n_2 \tilde{c}_{22}(q)} \right\}, \quad (21)$$

which exactly agrees with  $u_{11,MSA-PY}^{eff}(r)$  for the case of an original mixture of hard particles, where MSA and PY are equivalent. Thus, MSA-PY in Figs. 1 and 2 results from neglecting only the difference  $b_{11}^{eff}(r) - b_{11}(r)$ . Moreover, if we take RY instead of PY for the original mixture in (21), we obtain results for  $u_{11}^{eff}(r)$  which are still more accurate than  $u_{11,MSA-PY}^{eff}(r)$  (this result is not shown in Figs. 1 and 2). However, such improvement becomes relevant only close to the instability described by Eq. (15). The idea that  $u_{11}^{eff}(r)$  can be seen as a perturbation around  $u_{11}(r)$  has been used by several authors in the past and is well explained in Ref. [44] by following a rather different method than the one used in this paper.

HNC-PY, on the other hand, looks really bad in comparison with the simulation data. This can be understood by taking  $n_1 \rightarrow 0$  in Eq. (11), which together with Eq. (16) leads to  $\beta u_{11,HNC}^{eff}(r) = -\ln[1 + h_{11}(r)]$ . This agrees with the definition of the potential of mean force  $w_{11}(r)$  between particles of species 1 (note that this is no longer true for the concentrated systems). Therefore, the results for  $\beta u_{11,HNC-PY}^{eff}(r)$  shown in Figs. 1 and 2 correspond to the potential of the mean force obtained from PY, what we have corroborated by comparing  $\beta u_{11,HNC-PY}^{eff}(r)$  with  $-\ln[1 + h_{11}(r)]$ . Moreover, from Eqs. (11) and (13) we get

$$\beta u_{11}^{eff}(r) = \beta w_{11}(r) + n_1 \int_V c_{11}^{eff}(r') h_{11}(|\mathbf{r} - \mathbf{r}'|) d\mathbf{r}' + b_{11}^{eff}(r). \quad (22)$$

This result means that  $\beta u_{11}^{eff}(r)$  is given by  $\beta w_{11}(r)$  plus the correlation terms  $n_1 \int_V c_{11}^{eff}(r') h_{11}(|\mathbf{r} - \mathbf{r}'|) d\mathbf{r}' + b_{11}^{eff}(r)$ . If we neglect the bridge function we recover  $\beta u_{11,HNC}^{eff}(r)$  in the limit case  $n_1 \rightarrow 0$ . Thus, HNC-PY in Figs. 1 and 2 results from neglecting  $b_{11}^{eff}(r)$ . Moreover, the difference between  $\beta u_{11,HNC-PY}^{eff}(r)$  and the simulation data in those figures allows for the evaluation of  $b_{11}^{eff}(r)$ . This could be an efficient method to evaluate bridge functions through the effective interactions instead of the structure functions, which involve the inversion of the OZ equation and thereby introduce very large errors at small distances. We will, however, not report further in this direction at the moment.

In very diluted systems the virial-like expansion  $c_{ij}(r) = \sum_{\alpha, \beta, \dots, \gamma=0}^{\infty} n_1^{\alpha} n_2^{\beta} \dots n_p^{\gamma} c_{ij}^{(\alpha, \beta, \dots, \gamma)}(r)$  of the direct correlation functions can be made in Eq. (21). In the case of binary mixtures of hard spheres it leads to

$$\beta u_{11}^{eff}(r) = -n_2 \mathcal{F}^{-1} \{ \tilde{c}_{12}^{(0,0)}(q) \tilde{c}_{21}^{(0,0)}(q) \} \quad (23)$$

$$= -n_2 \int_V c_{12}^{(0,0)}(r') c_{21}^{(0,0)}(|\mathbf{r} - \mathbf{r}'|) d\mathbf{r}', \quad (24)$$

for  $n_1 \rightarrow 0$ , up to linear terms in  $n_2$ . Here, we used  $[1 - n_2 \tilde{c}_{22}(q)]^{-1} = 1 + n_2 \tilde{c}_{22}(q) + n_2^2 \tilde{c}_{22}^2(q) + \dots$  and the convolution theorem for Fourier transforms. In addition, it is known that [24]

$$\begin{aligned} c_{ij}^{(0,0)}(r) &= -1 \text{ for } r < \sigma_{ij} \\ &= 0 \text{ for } r \geq \sigma_{ij}. \end{aligned} \quad (25)$$

Equation (23), or Eq. (24), can also be obtained from Eq. (13), or from Eq. (16), by taking  $|h_{11}(r)| \ll 1$  (remember that we are trying with  $r \geq \sigma_1$ ) and neglecting  $b_{11}^{eff}(r)$ , as well as from Eq. (17). Following those routes we do need to take the additional approximation  $c_{11}^{(0,1)}(r) = 0$ . Moreover, the leading terms of the bridge functions are of quadratic order in the density [24] and, therefore, their exclusion of the dilute limit in our equations is exact. The integral in Eq. (24) accounts for the volume  $V_d$  of the region in the gap between the particles of species 1, separated by the distance  $r$ , from which the particles of species 2 are excluded due to their simultaneous overlap with both particles of species 1. This result can, therefore, be written as  $u_{11}^{eff}(r) = -(k_B T N_2 / V) V_d$ . Since the term in parenthesis corresponds to the pressure of an ideal gas composed of particles of species 2, the effective interaction potential is equivalent to the decrement of the free energy of the ideal gas when its volume is increased by  $V_d$ . This corresponds to the Asakura-Oosawa (AO) approximation for the depletion forces [1,2,8]. This result means that the dilute limit of our approach captures the exact dilute limit of the depletion interaction potential. In the following sections we generalize this result to mixtures of more than two components, as well as to nonspherical geometries, and use the symbol  $u_{11,AO}^{eff}(r)$  when working in that limit case.

As we can see from Eqs. (13) and (16)–(21), an evaluation of  $u_{11}^{eff}(r)$  requires a complete knowledge of the structure functions  $c_{ij}(r)$  and  $h_{ij}(r)$  of the original mixture. To proceed along these lines makes sense when the contraction of the description is imposed, for example, by experimental techniques unable to detect all the components. Then, Eqs. (13) and (16)–(21) allow for an interpretation of the results in terms of models including the experimentally “invisible” species. On the other hand, our approach apparently makes no sense when the goal of the contraction of the description is to simplify the mathematical problem. Fortunately, this is not the case. Apart from the lot we can learn about depletion forces just evaluating  $u_{11}^{eff}(r)$  in the cases in which the complete problem can be solved, we also find that simple approximations for  $c_{ij}(r)$  and  $h_{ij}(r)$  could lead to useful expressions for  $u_{11}^{eff}(r)$ . Equations (23) and (24), for example, do not use a precise input for  $c_{ij}(r)$  and  $h_{ij}(r)$ , and they still work fine for some cases in which the contracted particles are really not diluted, as we show in the next sections. Indeed, the generation of hierarchies, like the one defined by successive contractions of the description, is representative of the usual thinking of physicists working on many-body problems. This allows for simple approximations at a higher level of description which conduce to accurate results in a more reduced level of the hierarchy.

## V. BINARY AND TERNARY MIXTURES

Let us be very meticulous at the beginning of this section in order to explain the method of evaluating entropic potentials in the dilute limit. In a three-dimensional binary mixture

of hard spheres the Fourier transform of  $c_{12}^{(0,0)}(r)$  is [45]

$$\begin{aligned}\tilde{c}_{12}^{(0,0)}(q) &= \frac{4\pi}{q} \int_0^\infty rc_{12}^{(0,0)}(r)\sin(qr)dr \\ &= \frac{4\pi}{q^3} [q\sigma_{12} \cos(q\sigma_{12}) - \sin(q\sigma_{12})].\end{aligned}\quad (26)$$

Therefore, Eq. (23) takes the form

$$\begin{aligned}\beta u_{11,AO}^{eff}(r) &= -\frac{8n_2}{r} \int_0^\infty \frac{[q\sigma_{12} \cos(q\sigma_{12}) - \sin(q\sigma_{12})]^2}{q^5} \\ &\quad \times \sin(qr) dq,\end{aligned}\quad (27)$$

which can be analytically integrated to give

$$\beta u_{11,AO}^{eff}(r) = -\varphi_2 \left[ (\eta+1)^3 - \frac{3}{2}(\eta+1)^2 \frac{r}{\sigma_2} + \frac{1}{2} \frac{r^3}{\sigma_2^3} \right] \quad (28)$$

for  $\sigma_1 < r < \sigma_1 + \sigma_2$ , and 0 for larger distances. Here,  $\varphi_2 = \pi n_2 \sigma_2^3 / 6$  is the three-dimensional filling fraction of species 2, and  $\eta = \sigma_1 / \sigma_2$  the size ratio. The contact value is  $\beta u_{11,AO}^{eff}(\sigma_1^+) = -\varphi_2(1 + 3\eta/2)$ ; the depletion attraction increases either with  $\varphi_2$  or  $\eta$ . Equation (28) can also be obtained from Eq. (24), rewritten as

$$\begin{aligned}\beta u_{11,AO}^{eff}(r) &= -\frac{2\pi n_2}{r} \int_0^\infty c_{12}^{(0,0)}(r') dr' \int_{r-r'}^{r+r'} r'' c_{21}^{(0,0)}(r'') dr'' \\ &= -\frac{2\pi n_2}{r} \int_{r-\sigma_{12}}^{\sigma_{12}} dr' \int_{r-r'}^{\sigma_{12}} r'' dr'',\end{aligned}\quad (29)$$

or from a geometrical sketch by evaluating the volume  $V_d$  of the region in the gap between the particles of species 1 from which a particle of species 2 is excluded due to its simultaneous overlap with both particles of species 1, as done by Asakura and Oosawa [1,2]. The first expression in Eq. (29) is obtained by going to polar coordinates, after integrating over the angle [46]. The limits of integration in the second expression of Eq. (29) correspond to the simultaneous overlapping condition of a particle of species 2 with both particles of species 1, as required by Eq. (25).

In the special case seen in the previous paragraph the three routes, Eqs. (23) and (24), as well as the AO procedure, lead, more or less straightforwardly, to the analytical expression given in Eq. (28). However, the first two routes quickly lead to extremely complicated integrals, and the AO procedure becomes intractable, when trying with more sophisticated geometries. Nevertheless, Eq. (24) provides a numerical scheme which can be easily implemented in every case. By constructing an spatial grid around the overlapping region, we can check the simultaneous overlapping condition in every point of the grid. If the condition is fulfilled we add a volume element to the corresponding discretization of the integral in Eq. (24) and pass to the next point of the grid. In the opposite case, we only pass to the next point of the grid, and so forth. Let us now try this idea in the case of two-

dimensional binary mixtures of hard disks, where it is already hard to get an analytical expression for the integral involved in Eq. (23).

The Fourier transform of  $c_{12}^{(0,0)}(r)$  is [45]

$$\begin{aligned}\tilde{c}_{12}^{(0,0)}(q) &= 2\pi \int_0^\infty rc_{12}^{(0,0)}(r)J_0(qr)dr \\ &= 2\pi\sigma_{12} \frac{J_1(q\sigma_{12})}{q},\end{aligned}\quad (30)$$

where  $J_m(qr)$  is the Bessel function of order  $m$ . Equation (23) takes the form

$$\beta u_{11,AO}^{eff}(r) = -2\pi\sigma_{12}^2 n_2 \int_0^\infty \frac{J_0(qr)J_1^2(q\sigma_{12})}{q} dq. \quad (31)$$

We evaluate this integral numerically. The AO procedure allows in this case for a straightforward evaluation of  $V_d$ , leading to

$$\begin{aligned}\beta u_{11,AO}^{eff}(r) &= -\frac{2\varphi_2}{\pi} (1+\eta)^2 \left[ \cos^{-1}\left(\frac{1}{1+\eta\sigma_2} \frac{r}{\sigma_2}\right) \right. \\ &\quad \left. - \frac{1}{1+\eta\sigma_2} \frac{r}{\sigma_2} \sqrt{1 - \left(\frac{1}{1+\eta\sigma_2} \frac{r}{\sigma_2}\right)^2} \right]\end{aligned}\quad (32)$$

for  $\sigma_1 < r < \sigma_1 + \sigma_2$ , and 0 for larger distances. Here,  $\varphi_2 = \pi n_2 \sigma_2^2 / 4$  is the two-dimensional filling fraction of species 2, and  $\eta = \sigma_1 / \sigma_2$  the size ratio. We can also take the grid route by constructing a square grid of step  $\Delta = \sigma_2 / 10$  in order to evaluate numerically the integral in Eq. (24) in the form described in the previous paragraph. We also took  $\Delta = \sigma_2 / 20$ , but the result does not appreciably differ from the one obtained with the larger step. All routes lead to the same result, which corresponds to the dotted lines in Figs. 1 and 2. In some practical situations it should be convenient to have simple expressions for the potential at contact. In that case, Eq. (32) can be approximately written as  $\beta u_{11,AO}^{eff}(\sigma_1^+) \approx -(\varphi_2 / \pi) [1.89\eta^{1/2} + 0.66\eta^{-1/2} + \mathcal{O}(\eta^{-3/2})]$ . This is a very good approximation for  $\eta \geq 2$ .

From the Figs. 1 and 2 we can see that the dilute limit only captures the interaction potential in the range going from the contact,  $r = \sigma_1$ , to the case in which a particle of species 2 exactly fit in the gap between the two particles of species 1,  $r = \sigma_1 + \sigma_2$ . For larger distances the double overlap is not longer possible. That is also the reason why the AO limit does not capture the repulsive barrier growing in front of the attractive contact well. This barrier can only be explained including the effects of a second particle of species 2, which makes it possible for the formation of overlapping bridges between the particles of species 1 around the separation  $r = \sigma_1 + \sigma_2$ . We will come back to this point in Sec. IX. From Figs. 1 and 2 we can also see that the contact values of  $u_{11,HNC}^{eff}(r)$  and  $u_{11,AO}^{eff}(r)$  are very similar; both values considerably underestimate the depth of the depletion well at contact. However, they become very accurate for filling fractions  $\varphi_2$  of the order of 10%, or below it (this result is not shown in Figs. 1 and 2), which are values often met in experimental

situations. In the next sections we only use the grid route based on Eq. (24) in order to evaluate  $u_{11,AO}^{eff}(r)$ , but let us first work a little with ternary mixtures.

Up to this point we have assumed that we can only observe the particles of species 1 in a mixture of  $p$  spherical components. The other species are there, but we choose to ignore that fact. Therefore, we can describe the structure of the observed particles by means of the effective monodisperse OZ Eq. (11). Let us now assume that we can observe the particles of species 1 and 2 in the same mixture of  $p$  spherical components. In this new situation the contraction of Eq. (2) leads to the effective OZ equation for a binary mixture,

$$\tilde{h}_{\alpha\beta}(q) = \tilde{c}_{\alpha\beta}^{eff}(q) + \sum_{\gamma=1}^2 n_{\gamma} \tilde{c}_{\alpha\gamma}^{eff}(q) \tilde{h}_{\gamma\beta}(q), \quad (33)$$

written here in the Fourier space. The effective direct correlation function  $\tilde{c}_{\alpha\beta}^{eff}(q)$  is found to be given by

$$\begin{aligned} \tilde{c}_{\alpha\beta}^{eff}(q) = & \tilde{c}_{\alpha\beta}(q) + \sum_{i \neq \alpha, \beta}^p \frac{\tilde{c}_{\alpha i}(q) n_i \tilde{c}_{i\beta}(q)}{[1 - n_i \tilde{c}_{ii}(q)]} \\ & + \sum_{i \neq \alpha, \beta}^p \sum_{j \neq \alpha, \beta, i}^p \frac{\tilde{c}_{\alpha i}(q) n_i \tilde{c}_{ij}(q) n_j \tilde{c}_{j\beta}(q)}{[1 - n_i \tilde{c}_{ii}(q)][1 - n_j \tilde{c}_{jj}(q)]} + \dots \end{aligned} \quad (34)$$

Here, the greek indexes run over the observed species, i.e.,  $\alpha, \beta = 1, 2$ . The  $c_{11}^{eff}(r)$  from Eq. (12) does not correspond to the  $c_{11}^{eff}(r)$  from Eq. (34), since the first one is a more contracted member of the hierarchy than the latter. The first one can be obtained after the contraction of species 2 in Eq. (33), which leads to Eq. (18), but having the structure functions of Eq. (33) as input. By using (34) in those expressions, Eq. (12) can be recovered. To proceed along these lines allows for the generation of hierarchies defined by successive contractions of the description. However, in this paper we no longer report on that question.

In the special case of ternary mixtures we can choose from the contraction of two components, or of only one. If we contract two components we get Eqs. (11) and (12) again, but with  $p=3$ , which add some terms to Eq. (18). The contraction of only one component corresponds to the case described by Eqs. (33) and (34), in which two species can be observed. In that case, the effective crossed interaction potential is given by

$$\beta u_{12}^{eff}(r) = \beta u_{12}(r) - n_3 \mathcal{F}^{-1} \left\{ \frac{\tilde{c}_{13}(q) \tilde{c}_{32}(q)}{1 - n_3 \tilde{c}_{33}(q)} \right\}, \quad (35)$$

if we neglect the difference between the crossed bridge functions  $b_{12}^{eff}(r) - b_{12}(r)$ . In the case of systems composed of hard particles, in the infinite dilute limit of observable species,  $n_1 \rightarrow 0$  and  $n_2 \rightarrow 0$ , up to linear terms in the density of the contracted species,  $n_3$ , we get

$$\beta u_{12,AO}^{eff}(r) = -n_3 \mathcal{F}^{-1} \{ \tilde{c}_{13}^{(0,0)}(q) \tilde{c}_{32}^{(0,0)}(q) \} \quad (36)$$

$$= -n_3 \int_V c_{13}^{(0,0)}(r') c_{32}^{(0,0)}(|\mathbf{r} - \mathbf{r}'|) d\mathbf{r}'. \quad (37)$$

The integral in Eq. (37) accounts for the volume  $V_d$  of the region in the gap between two particles of species 1 and 2, separated by the distance  $r$ , from which a particle of species 3 is excluded due to its simultaneous overlap with both particles of species 1 and 2. Thus, the dilute limit in our equations also captures the AO approximation in the case of ternary mixtures.

In three-dimensional systems Eqs. (36) and (37) can be analytically evaluated to give [8]

$$\begin{aligned} \beta u_{12,AO}^{eff}(r) = & -\varphi_3 \left[ (\bar{\eta} + 1)^3 - \frac{3}{2} (\bar{\eta} + 1)^2 \frac{r}{\sigma_3} + \frac{1}{2} \frac{r^3}{\sigma_3^3} \right] \\ & + \frac{3\varphi_3}{8(r/\sigma_3)} (\eta_1 - \eta_2)^2 \left[ (\bar{\eta} + 1) - \frac{r}{\sigma_3} \right]^2 \end{aligned} \quad (38)$$

for  $\sigma_{12} < r < \sigma_{12} + \sigma_3$ , and 0 for larger distances. Here,  $\eta_i = \sigma_i / \sigma_3$  and  $\bar{\eta} = (\eta_1 + \eta_2) / 2$ . This result can also be straightforwardly obtained from the AO procedure. The contact value of Eq. (38) is  $\beta u_{12,AO}^{eff}(\sigma_{12}^+) = -\varphi_3 [1 + 3\eta_1 \eta_2 / (\eta_1 + \eta_2)]$ . Therefore, at fixed  $\eta_2$ , the depletion attraction increases with  $\eta_1$  up to the asymptotic value  $\beta u_{12,AO}^{eff}(\sigma_{12}^+) = -\varphi_3 (1 + 3\eta_2)$  when  $\eta_1 \rightarrow \infty$ . As we will see in the next section, this case corresponds to a binary mixture in front of a flat hard wall.

In two-dimensional systems Eq. (36) becomes

$$\beta u_{12,AO}^{eff}(r) = -2\pi\sigma_{13}\sigma_{32}n_3 \int_0^\infty \frac{J_0(qr)J_1(q\sigma_{13})J_1(q\sigma_{32})}{q} dq. \quad (39)$$

We evaluate this integral numerically. The AO procedure allows also in this case for a straightforward evaluation of  $V_d$ , leading to

$$\begin{aligned} \beta u_{12,AO}^{eff}(r) = & -\frac{\varphi_3}{\pi} (1 + \eta_1)^2 \left[ \cos^{-1} \left( \frac{r_1}{1 + \eta_1} \right) \right. \\ & \left. - \frac{r_1}{1 + \eta_1} \sqrt{1 - \left( \frac{r_1}{1 + \eta_1} \right)^2} \right] \\ & - \frac{\varphi_3}{\pi} (1 + \eta_2)^2 \left[ \cos^{-1} \left( \frac{r_2}{1 + \eta_2} \right) \right. \\ & \left. - \frac{r_2}{1 + \eta_2} \sqrt{1 - \left( \frac{r_2}{1 + \eta_2} \right)^2} \right], \end{aligned} \quad (40)$$

for  $\sigma_{12} < r < \sigma_{12} + \sigma_3$ , and 0 for larger distances. Here,  $r_1 = (\sigma_3/4r)[4(r/\sigma_3)^2 + (1 + \eta_1)^2 - (1 + \eta_2)^2]$  and  $r_2 = (2r/\sigma_3) - r_1$ . We also take the grid route based on Eq. (37) by constructing a square grid of step  $\Delta = \sigma_3/10$ . All routes lead to the same results, which correspond to the dotted lines in Fig. 3. The depletion attraction increases with  $\eta_1$ , at fixed  $\eta_2$ , until reaching the asymptotic value corresponding to a flat hard wall when  $\eta_1 \rightarrow \infty$ . Indeed,  $u_{12,AO}^{eff}(r)$  can be interpreted as the depletion interaction potential between a convex hard wall of

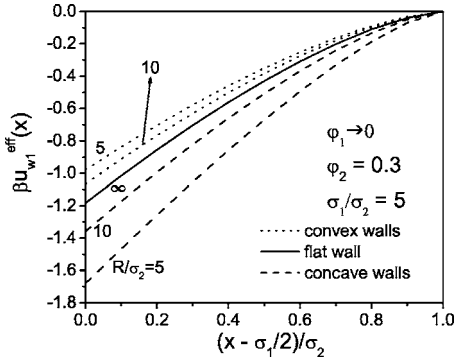


FIG. 3. The figure shows the wall-particle depletion potential  $\beta u_{w1,AO}^{eff}(x)$  for a two-dimensional binary mixture of hard disks in the dilute limit in our equations. The dotted lines correspond to the case of convex hard walls with scaled radius of curvature  $R/\sigma_2 = 5$  and 10. They can also be interpreted as the dilute limit of the effective interaction potential  $\beta u_{12,AO}^{eff}(r)$  in a homogeneous ternary mixture of hard disks with  $\sigma_2 \rightarrow \sigma_3$ ,  $\sigma_1 \rightarrow \sigma_2$ ,  $2R \rightarrow \sigma_1$ , and  $x + \sigma_1/2 \rightarrow r$  (see Sec. V). The full line corresponds to the case of a hard flat wall ( $R \rightarrow \infty$ ), and the dashed lines to the case of concave hard walls with scaled radius of curvature  $R/\sigma_2 = 5$  and 10. The parameters of the binary mixture in front of the walls are  $\phi_1 \rightarrow 0$ ,  $\phi_2 = 0.3$ , and  $\sigma_1/\sigma_2 = 5$ .

radius of curvature  $\sigma_1/2$  and particles of species 2 immersed in a bath of smaller particles of species 3. We try further with wall effects in the next section.

## VI. IN FRONT OF A HARD WALL

The concentration profile of a colloidal mixture of  $p$  spherical components in front of a wall is described by the inhomogeneous OZ equation [24],

$$\tilde{h}_{wi}(\mathbf{q}) = \tilde{c}_{wi}(\mathbf{q}) + \sum_{j=1}^p n_j \tilde{h}_{wj}(\mathbf{q}) \tilde{c}_{ji}(q), \quad (41)$$

which has to be complemented with a closure relation of the general form [24]

$$c_{wi}(\mathbf{r}) = -\beta u_{wi}(\mathbf{r}) + h_{wi}(\mathbf{r}) - \ln[1 + h_{wi}(\mathbf{r})] + b_{wi}(\mathbf{r}). \quad (42)$$

Here,  $h_{wi}(\mathbf{r})$  is the wall-particle total correlation function,  $c_{wi}(\mathbf{r})$  the wall-particle direct correlation function,  $u_{wi}(\mathbf{r})$  the wall-particle interaction potential,  $b_{wi}(\mathbf{r})$  the wall-particle bridge function, and  $c_{ij}(r)$  the same direct correlation function of the bulk suspension appearing in Eqs. (2) and (3). The wall-particle structure functions depend on the positional vector  $\mathbf{r}$  and, therefore, their Fourier transforms on the wave vector  $\mathbf{q}$ , since the wall breaks the isotropy of the system. The properties of Eqs. (41) and (42) have been carefully studied in a series of papers published in the last ten years, for systems of charged and uncharged components [47–51]. We will use here their invariance under contractions of the description in order to get the effective wall-particle interaction potential in systems composed of hard colloidal particles in front of a hard wall.

If we assume that we can only see the wall and the particles of species 1, the concentration profile of this species in front of the wall is described by the effective monodisperse inhomogeneous OZ equation [11]

$$\tilde{h}_{w1}(\mathbf{q}) = \tilde{c}_{w1}^{eff}(\mathbf{q}) + n_1 \tilde{h}_{w1}(\mathbf{q}) \tilde{c}_{11}^{eff}(q), \quad (43)$$

with

$$\begin{aligned} \tilde{c}_{w1}^{eff}(\mathbf{q}) = & \tilde{c}_{w1}(\mathbf{q}) + \sum_{i \neq 1}^p \frac{\tilde{c}_{wi}(\mathbf{q}) n_i \tilde{c}_{i1}(q)}{[1 - n_i \tilde{c}_{ii}(q)]} \\ & + \sum_{i \neq 1}^p \sum_{j \neq 1, i}^p \frac{\tilde{c}_{wi}(\mathbf{q}) n_i \tilde{c}_{ij}(q) n_j \tilde{c}_{j1}(q)}{[1 - n_i \tilde{c}_{ii}(q)][1 - n_j \tilde{c}_{jj}(q)]} + \dots \end{aligned} \quad (44)$$

and  $\tilde{c}_{11}^{eff}(q)$  is given by Eq. (12). The other species are there, but we choose to ignore that fact, which is exactly what forces us to develop an effective description of the system. In the case of binary mixtures Eq. (44) leads to [neglecting the difference  $b_{w1}^{eff}(\mathbf{r}) - b_{w1}(\mathbf{r})$ ]

$$\beta u_{w1}^{eff}(\mathbf{r}) = \beta u_{w1}(\mathbf{r}) - n_2 \mathcal{F}^{-1} \left\{ \frac{\tilde{c}_{w2}(\mathbf{q}) \tilde{c}_{21}(q)}{1 - n_2 \tilde{c}_{22}(q)} \right\}, \quad (45)$$

and, therefore, to

$$\beta u_{w1,AO}^{eff}(\mathbf{r}) = -n_2 \mathcal{F}^{-1} \{ \tilde{c}_{w2}^{(0,0)}(\mathbf{q}) \tilde{c}_{21}^{(0,0)}(q) \} \quad (46)$$

$$= -n_2 \int_V c_{w2}^{(0,0)}(\mathbf{r}') c_{21}^{(0,0)}(|\mathbf{r} - \mathbf{r}'|) d\mathbf{r}' \quad (47)$$

in systems of hard particles, in the infinite dilute limit of species 1,  $n_1 \rightarrow 0$ , up to linear terms in  $n_2$ . As it can be seen from Eq. (47), the AO approximation is again captured by the dilute limit of our equations. Equation (46) is still more complicated to evaluate than Eq. (23), due to its dependence on the wave vector. In the case of flat hard walls, however, Eq. (47) and the AO procedure allow for a straightforward evaluation of  $u_{w1,AO}^{eff}(\mathbf{r})$ , which leads to

$$\beta u_{w1,AO}^{eff}(x) = -\varphi_2 (1 + 3\eta) \left( \frac{3}{2} - \frac{x}{\sigma_2} \right)^2 \quad (48)$$

in three-dimensional systems, and to

$$\begin{aligned} \beta u_{w1,AO}^{eff}(x) = & -\frac{\varphi_2}{2\pi} (1 + \eta)^2 \\ & \times \left[ \pi + 2 \tan^{-1} \left( \frac{1 - 2x/\sigma_2}{\sqrt{(1 + \eta)^2 - (1 - 2x/\sigma_2)^2}} \right) \right] \\ & - \frac{\varphi_2}{\pi} (1 - 2x/\sigma_2) \sqrt{(1 + \eta)^2 - (1 - 2x/\sigma_2)^2} \end{aligned} \quad (49)$$

in two-dimensional systems, both for  $\sigma_1/2 < x < \sigma_1/2 + \sigma_2$  and 0 for larger distances. Here,  $\eta = \sigma_1/\sigma_2$  and  $x$  is the distance between the surface of the wall and the center of particles of species 1. The contact values are

$\beta u_{w1,AO}^{eff}(\sigma_1^+/2) = -\varphi_2(1+3\eta)$  and  $\beta u_{w1,AO}^{eff}(\sigma_1^+/2) = -(16\varphi_2/15\pi)(1+5\eta)\eta^{-1/2}$  for  $\eta \geq 2$ , respectively. Equations (48) and (49) can also be obtained from the limit  $\eta_1 \rightarrow \infty$ , at fixed  $\eta_2$ , of Eqs. (38) and (40), respectively. The result for the two-dimensional case is shown in Fig. 3 by the full line for a binary mixture with  $\varphi_2=0.3$ , and  $\sigma_1/\sigma_2=5$ . The depletion attraction increases with the radius of curvature  $R$  of the convex walls, reaching an extreme value for flat walls ( $R \rightarrow \infty$ ).

We now consider binary mixtures of hard spheres in front of concave hard walls of radius of curvature  $R$  in the dilute limit. Although it is possible to get an analytical expression for  $u_{w1,AO}^{eff}(x)$  also in this case, we prefer to work in the following with the numerical evaluation of Eq. (47) by constructing a square grid of step  $\Delta = \sigma_2/10$  around the double overlapping region. In the case of two-dimensional systems the latter is defined by the conditions

$$R - \sqrt{x_2^2 + y_2^2} < \frac{\sigma_2}{2}$$

$$\sqrt{(x_2 + x - R)^2 + y_2^2} < \sigma_{12}, \quad (50)$$

which have to be fulfilled simultaneously. Here,  $(x_2, y_2)$  and  $(R-x, 0)$  are the coordinates of the particles of species 2 and 1, respectively, referred to the center of curvature of the concave wall. We check the overlapping conditions (50) in every point of the grid. If both conditions are fulfilled simultaneously we add a volume element to the integral in Eq. (47). In the opposite case, we pass to the next point of the grid. The results obtained by this way are shown in Fig. 3 by the dashed lines. As we can see from that figure, the more concave the wall, the larger the depletion attraction.

The previous results indicate that the suspended particles in front of a wall are pushed to the wall due to the depletion interaction, and that the amplitude of such interaction can be manipulated by changing the parameters of the suspension, such as particle size and concentration, and of the wall, such as its curvature. This occurs although we are working with hard particles and hard walls, whose interaction is only repulsive and short-ranged. The origin of the long-ranged depletion forces is that the system increases its entropy when the larger particles are placed close to the wall, letting free the volume of the bulk for the smaller particles, which are very much more numerous. Moreover, the entropy of the smaller particles may become still larger when the larger particles are put in an ordered array. Indeed, this phenomenon has been already used in order to generate self-assembled structures, as in the crystallization of protein suspensions [52] or in the selective adsorption of colloidal particles on structured walls [53,54]. Regarding the latter, there is strong evidence for nonadsorption of hard spheres on flat hard walls [47–51]. However, as we will see in the next section, the situation looks very different when the wall has a relief pattern.

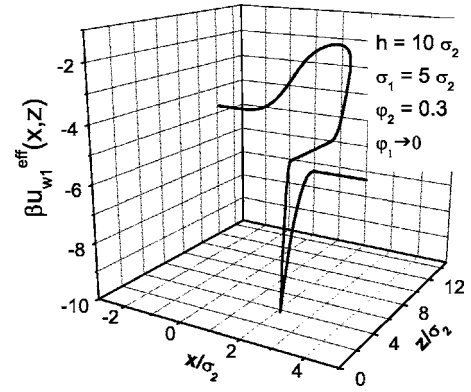


FIG. 4. The figure shows the contact wall-particle depletion potential  $\beta u_{w1,AO}^{eff}(x, z)$  for a binary mixture of hard spheres, in the dilute limit, in front of a hard wall with a linear step edge of height  $h = 10\sigma_2$  along the  $y$  axis. The upper level of the step is in the region with  $x < 0$  and  $z = h$ , on a plane parallel to the  $xy$  plane, and the lower level in the region with  $x > 0$  and  $z = 0$ , on the  $xy$  plane. The parameters of the binary mixture in front of the wall are  $\varphi_1 \rightarrow 0$ ,  $\varphi_2 = 0.3$ , and  $\sigma_1/\sigma_2 = 5$ .

## VII. SURFACES OF ENTROPIC POTENTIAL

When the walls have a relief pattern combining concave and convex regions the depletion potential at contact defines a potential landscape that we will call here surface of entropic potential. One of the simplest cases, in which we can calculate this property, is when an otherwise flat wall has a linear step edge of height  $h$  along the  $y$ -axis. Let us consider a hard wall with a step edge of height  $h = 10\sigma_2$ , and, in front of it, a binary mixture of hard spheres with parameters  $\varphi_1 \rightarrow 0$ ,  $\varphi_2 = 0.3$ , and  $\sigma_1/\sigma_2 = 5$ . These values are the same as in Fig. 3, but a direct comparison is not possible since we are trying with a three-dimensional system this time. The upper level of the step is in the region with  $x < 0$  and  $z = h$ , on a plane parallel to the  $xy$ -plane, and the lower level in the region with  $x > 0$  and  $z = 0$ , on the  $xy$ -plane. Note that the meaning of the variable  $x$  differs from the one previously used in this paper.

In the infinite dilute limit of particles of species 1, up to linear terms in  $n_2$ , the wall-particle depletion potential is given by Eq. (47), with the appropriate overlapping conditions for  $c_{w2}^{(0,0)}(\mathbf{r})$  and  $c_{12}^{(0,0)}(r)$ . In order to evaluate this equation at contact we follow the grid route by constructing a cubic grid of step  $\Delta = \sigma_2/10$  over the wall. Then, we check in every point of the grid the condition of simultaneous overlapping of a particle of species 2 with the wall and with a particles of species 1 always in contact with the wall. The latter is then moved along the  $x$ -axis in order to scan the region around the step edge. The results we found for  $\beta u_{w1,AO}^{eff}(x, z)$  are shown in Fig. 4. The line represents a contact scanning of the wall, beginning on the upper level and ending on the lower level of the step. Far away from the edge the scanning particle only see a flat wall and, therefore, the value  $\beta u_{w1,AO}^{eff}(x \leq 0, h) = \beta u_{w1,AO}^{eff}(x \geq 0, 0) = -4.8$  can be also obtained from the contact limit of Eq. (48). Closing the edge from the left, the scanning particle first feels a force opposite to its motion, parallel to the wall, and a some weaker attrac-

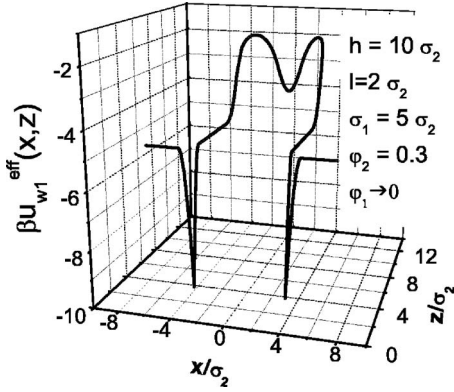


FIG. 5. The figure shows the contact wall-particle depletion potential  $\beta u_{w1,AO}^{eff}(x,z)$  for a binary mixture of hard spheres, in the dilute limit, in front of a hard wall with a linear barrier of height  $h=10\sigma_2$  and thickness  $l=2\sigma_2$  along the  $y$  axis. The top of the barrier is in the region with  $-\sigma_2 < x < \sigma_2$  and  $z=h$ , on a plane parallel to the  $xy$  plane, and the rest of the wall in the region with  $x < -\sigma_2$ , or  $x > \sigma_2$ , and  $z=0$ , on the  $xy$  plane. The parameters of the binary mixture in front of the wall are  $\varphi_1 \rightarrow 0$ ,  $\varphi_2=0.3$ , and  $\sigma_1/\sigma_2=5$ .

tion perpendicular to the wall. Those features arise from the collisions with the smaller spheres in front of the lower level of the step and in the neighborhood of the edge. After crossing this region, the scanning particle falls into a very attractive well located on the concave edge of the step. In order to leave this well the particle has to move against a force, parallel to the wall, pushing it back to the concave edge. Some of these predictions have been already observed in the lab [53]. It has also been shown that the attractive well at the concave edge could lead to the selective deposition of particles [54]. Our results are in quantitative agreement with the experimental data.

We now repeat the same calculation, but for a hard wall with a linear barrier of height  $h=10\sigma_2$  and thickness  $l=2\sigma_2$  along the  $y$ -axis. The top of the barrier is in the region with  $-\sigma_2 < x < \sigma_2$  and  $z=h$ , on a plane parallel to the  $xy$ -plane, and the rest of the wall in the region with  $x < -\sigma_2$ , or  $x > \sigma_2$ , and  $z=0$ , on the  $xy$ -plane. In Fig. 5 we show the contact value of the dilute limit of the wall-particle depletion potential for the same binary mixture of Fig. 4. The line represents a contact scanning of the wall, beginning on the left side of the barrier ( $x < -\sigma_2$ ;  $z=0$ ), climbing up, crossing the barrier ( $-\sigma_2 < x < \sigma_2$ ;  $z=h$ ), going down, and ending on the other side ( $x > \sigma_2$ ;  $z=0$ ). Most of the features of this potential can be understood as a superposition of two opposite lying step edges. Nevertheless, at the center of the top of the barrier a second attractive well is developed, which could trap the particles in both directions, parallel and perpendicular to the wall. This may also lead to selective adsorption of colloidal particles in one-dimensional crystal arrays.

The cases investigated above show that the geometry of the wall plays a very important role in the behavior of the wall-particle depletion potential. Indeed, Eq. (47) allows for the design of surfaces of entropic potential by just choosing the geometrical features of the wall, and/or the parameters of the suspension. Basically, this means that the entropy of the system can be manipulated in order to induce a wished struc-

ture in a part of it. We will report further about this issue in a future paper. For the moment, let us please investigate what happens when the depleting particles are no longer spherical.

## VIII. CONTRACTION OF THE GEOMETRY

The contraction of the description procedure we have developed for homogeneous mixtures of spherical particles in the previous sections can be straightforwardly extended to the case of homogeneous mixtures of nonspherical particles, whose structure is given by the orientation dependent Ornstein-Zernike equation [24]

$$h_{ij}(\mathbf{r}_{12}, \mathbf{u}_1, \mathbf{u}_2) = c_{ij}(\mathbf{r}_{12}, \mathbf{u}_1, \mathbf{u}_2) + \sum_{k=1}^p \frac{n_k}{\Omega} \int_V \int_{\Omega} d\mathbf{r}_3 d\mathbf{u}_3 \times c_{ik}(\mathbf{r}_{13}, \mathbf{u}_1, \mathbf{u}_3) h_{kj}(\mathbf{r}_{32}, \mathbf{u}_3, \mathbf{u}_2), \quad (51)$$

as we have already reported in a previous paper [17]. We illustrate here this idea for a binary mixture of spherical and nonspherical hard particles by assuming that the spherical particles are the observed species, indexed as species 1. The contraction of the nonspherical species, indexed as species 2, leads then to the effective OZ equation

$$h_{11}(r_{12}) = c_{11}^{eff}(r_{12}) + n_1 \int_V d\mathbf{r}_3 c_{11}^{eff}(r_{13}) h_{11}(r_{32}) \quad (52)$$

with

$$c_{11}^{eff}(r_{12}) = c_{11}(r_{12}) + \frac{n_2}{\Omega} \int_V \int_{\Omega} d\mathbf{r}_3 d\mathbf{u}_3 c_{12}(\mathbf{r}_{13}, \mathbf{u}_3) c_{21}(\mathbf{r}_{32}, \mathbf{u}_3) + \dots \quad (53)$$

The functions  $h_{ij}(\mathbf{r}_{12}=\mathbf{r}_2-\mathbf{r}_1, \mathbf{u}_1, \mathbf{u}_2)$  and  $c_{ij}(\mathbf{r}_{12}, \mathbf{u}_1, \mathbf{u}_2)$  in Eq. (51) are the total and direct correlation functions between a particle of species  $i$  with its center of mass at  $\mathbf{r}_1$  and orientational vector  $\mathbf{u}_1$ , and a particle of species  $j$  with its center of mass at  $\mathbf{r}_2$  and orientational vector  $\mathbf{u}_2$ . The quantity  $\Omega$  refers to the total solid angle;  $4\pi$  for three-dimensional systems, and  $2\pi$  for two-dimensional systems. For spherical particles the structure functions only depend on the distance  $r_{12}=|\mathbf{r}_{12}|$  between particles. Equation (53) corresponds to Eq. (18), but is written in the real space. The points  $\dots$  stand for all the terms not explicitly given, which are of quadratic and higher order in  $n_2$ .

In the infinite dilute limit of particles of species 1, up to linear terms in  $n_2$ , the depletion potential is given by

$$\beta u_{11,AO}^{eff}(r_{12}) = -\frac{n_2}{\Omega} \int_V \int_{\Omega} d\mathbf{r}_3 d\mathbf{u}_3 c_{12}^{(0,0)}(\mathbf{r}_{13}, \mathbf{u}_3) c_{21}^{(0,0)}(\mathbf{r}_{32}, \mathbf{u}_3) \quad (54)$$

where the correlation functions  $c_{12}^{(0,0)}(\mathbf{r}_{13}, \mathbf{u}_3)$  and  $c_{21}^{(0,0)}(\mathbf{r}_{32}, \mathbf{u}_3)$  between spherical and nonspherical particles are  $-1$  when both particles overlap and  $0$  elsewhere. As in the previous sections, Eq. (54) can also be written as  $\beta u_{11,AO}^{eff}(r) = -n_2 V_d$ , with  $V_d$  being the volume of the region in the gap between two particles of species 1, separated by the

TABLE I. The table shows the contact value  $\beta u_{11,AO}^{eff}(\sigma_1^+)$  for three different binary mixtures composed of large hard spheres of diameter  $\sigma_1$  with additional (I) small hard spheres of diameter  $\sigma_2$ , (II) small spherocylinders of diameter  $\sigma_2$  and length  $\sigma_2+L$ , and (III) small hard spheres of diameter  $\sigma_2+L$ . The other parameters are  $\sigma_1=10\sigma_2$  and  $L=5\sigma_2$ .

$\varphi_2$	$\beta u_{11,AO}^{eff}(\sigma_1^+)$		
	I	II	III
0.01	-0.16	-0.2453	-0.035
0.02	-0.32	-0.4906	-0.070
0.03	-0.48	-0.7359	-0.105

distance  $r$ , from which the particles of species 2 are excluded due to their simultaneous overlap with both particles of species 1. After assuming that the nonspherical particles are hard spherocylinders of diameter  $\sigma_2$  and length  $\sigma_2+L$ , we evaluate the integral in Eq. (54) by following the grid route, i.e., by constructing a spatial grid around the overlapping region. Spatial grid steps of  $0.001\sigma_2$  and angular grid steps of  $1^\circ$  provide accurate values for  $\beta u_{11,AO}^{eff}(r)$  (up to the third significant digit). Since we are working with three-dimensional systems we take  $\Omega=4\pi$  in our equations.

One is tempted to think that the depletion attraction produced by the spherocylinders should be somewhere between the one due to small spheres of diameter  $\sigma_2$  and the one due to small spheres of diameter  $\sigma_2+L$ . Therefore, in order to understand how the entropic potential change due to the geometry of the contracted particles, we first compare in Table I the contact value  $\beta u_{11,AO}^{eff}(\sigma_1^+)$  for three different binary mixtures composed of large hard spheres of diameter  $\sigma_1$  with additional (I) small hard spheres of diameter  $\sigma_2$ , (II) small spherocylinders of diameter  $\sigma_2$  and length  $\sigma_2+L$ , and (III) small hard spheres of diameter  $\sigma_2+L$ . We identify those systems in our notation with the indexes I–III, respectively. The corresponding volume fractions are  $\varphi_2=\pi n_2\sigma_2^3/6$ ,  $\varphi_2=\pi n_2\sigma_2^3(1+3L/2\sigma_2)/6$ , and  $\varphi_2=\pi n_2\sigma_2^3(1+L/\sigma_2)^3/6$ . We use  $\sigma_1=10\sigma_2$  and  $L=5\sigma_2$ , take care of being well below the critical volume fraction in which two rotating spherocylinders partially overlap, and assume the same volume fraction for the three mixtures, which implies different number densities. Surprisingly, the larger attractions are produced by the spherocylinders, although the number density  $n_2$  in model I is 8.5 times larger than in model II. This results alone from the larger values of  $V_d$  for nonspherical particles. In the systems of Table I, for example, the value of  $V_d$  at contact for spherocylinders is approximately 13.032 times larger than the one for small spheres of diameter  $\sigma_2$ .

The effect of the geometry of the depleting agent can also be appreciated in Fig. 6, where we show  $V_d(r)$  for six mixtures of the type II with  $\sigma_1=10\sigma_2$  and several values of  $L$ , ranging from 0 (model I) to  $5\sigma_2$ . The corresponding entropic potential will show basically the same qualitative behavior as in the case of mixtures of spheres, but it will be more attractive at contact and more long-ranged. The volume  $V_d(r)$

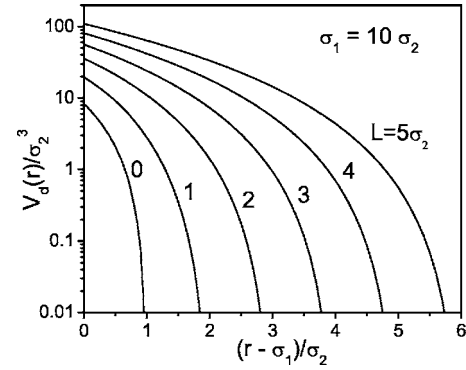


FIG. 6. The figure shows the double overlapping volume  $V_d(r)$  for six mixtures of large hard spheres of diameter  $\sigma_1$  and small spherocylinders of diameter  $\sigma_2$  and length  $\sigma_2+L$ . The other parameters are  $\sigma_1=10\sigma_2$ , and  $L$  ranges from 0 to  $5\sigma_2$ .

becomes zero first when a spherocylinder, positioned along the line connecting the centers of the large spheres, exactly fits the gap between them, i.e., at  $r=\sigma_1+\sigma_2+L$ . The volume of double overlapping increases very fast with  $L$ . This effect should produce a phase separation in the suspension of spherical and nonspherical particles at smaller volume fractions than in the case of a binary mixture of hard spheres. Moreover, it is straightforward to show that Eq. (54) recovers the case with  $\sigma_2=0$  (binary mixture of hard spheres and hard needle-like particles) which has been reported by other authors [55,56]. In general our results agree with experimental data [57].

It is often the belief that the deeper attraction produced by rod-like particles is due to the rotational contributions to the entropy of the system. From Eq. (54) it can be seen, however, that it is not the case in the AO limit. This equation can be written as  $u_{11,AO}^{eff}(r)=-k_B T N_2/V V_d$ . The term in parenthesis is an ideal gas property, which does depend on the translational degrees of freedom, but not on the rotational degrees of freedom. The volume  $V_d$  is a pure geometric property, which does not depend on the dynamics of the particles. The rotational contributions to the entropy become really relevant only with increasing volume fractions, due to the correlations between rod-like particles, which are neglected in Eq. (54) [17].

## IX. CONCENTRATION EFFECTS AND ENERGETIC CONTRIBUTIONS

When the concentration of depleting particles increases, the attractive well at contact becomes deeper and a potential barrier develops in front of it, followed by a secondary well, as shown in Figs. 1 and 2. This is due to the correlations between the contracted particles, which are not included in AO. In order to include them in our equations, we expand, in Eq. (21), the direct correlation functions in the virial-like form  $c_{ij}(r)=\sum_{\alpha,\beta=0}^{\infty} n_1^\alpha n_2^\beta c_{ij}^{(\alpha,\beta)}(r)$  and get the following expression for the depletion potential:

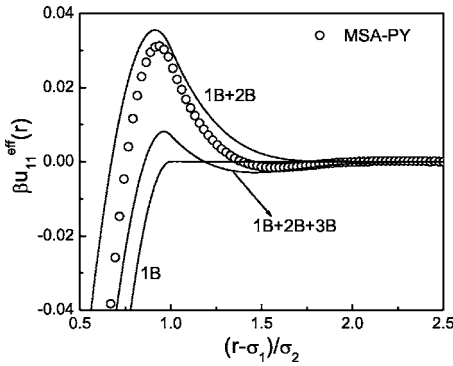


FIG. 7. The figure shows the single bridges  $1B$ , double bridges  $2B$ , and triple bridges  $3B$  contributions to the depletion potential in a mixture of hard spheres with  $\sigma_1=10\sigma_2$ ,  $\varphi_2=0.05$ , and  $\varphi_1 \rightarrow 0$ . Those results are compared to the MSA-PY approximation (open circles).

$$\begin{aligned} \beta u_{11}^{eff}(r) = & \beta u_{11}(r) - n_2 \mathcal{F}^{-1} \{ \tilde{c}_{12}^{(0,0)}(q) \tilde{c}_{21}^{(0,0)}(q) \} \\ & - n_2^2 \mathcal{F}^{-1} \{ \tilde{c}_{12}^{(0,0)}(q) \tilde{c}_{22}^{(0,0)}(q) \tilde{c}_{21}^{(0,0)}(q) \} \\ & - n_2^3 \mathcal{F}^{-1} \{ \tilde{c}_{12}^{(0,0)}(q) \tilde{c}_{22}^{(0,0)}(q) \tilde{c}_{22}^{(0,0)}(q) \tilde{c}_{21}^{(0,0)}(q) \} + \dots, \end{aligned} \quad (55)$$

where we neglected the functions  $c_{12}^{(0,1)}(r)$  and  $c_{12}^{(0,2)}(r)$  in the terms of quadratic and cubic order in  $n_2$ . Thus, the first term [after the naked potential  $\beta u_{11}(r)$ ], which corresponds to the AO approximation and is denoted by  $1B$  in this section, can be interpreted as representing single bridges between two particles of species 1 formed by a particle of species 2. The second term, which we will denote here by  $2B$ , represents the bridges between two particles of species 1 formed by two particles of species 2. The third term, denoted by  $3B$ , represents triple bridges formed by two particles of species 1 and three particles of species 2 in between, and so forth.

We evaluate the first terms of Eq. (55) for a binary mixture of hard spheres with  $\sigma_1=10\sigma_2$ ,  $\varphi_2=0.05$ , and  $\varphi_1 \rightarrow 0$  in order to study how the correlations between the contracted particles determine the form of the interaction potential between the observable particles. In Fig. 7 we show that the term  $1B$  leads to the depletion attraction at contact, as we already knew from the previous sections. The double bridges, or term  $2B$ , lead to the repulsive barrier in front of the attractive well at contact, as shown in Fig. 7 by the sum  $1B+2B$ . Moreover, the triple bridges produce the secondary attraction in front of the repulsive barrier, as shown by the sum  $1B+2B+3B$ . The open circles were obtained from the MSA-PY approximation and are expected to be very close to the real depletion potential due to the small value of the volume fraction.

The correlations between the contracted particles become relevant when the concentration of one or more species increases, as well as when one or more species are interacting with longer ranged potentials than the hard core. Indeed, depletion forces can be strongly affected if van der Waals or Coulombic interactions are present in the system. As shown in Fig. 7, if we want to capture such concentration effects and energetic contributions we have to go beyond the AO approximation. The form in which we did it in Fig. 7, how-

ever, is only useful to understand the way in which those correlations will affect our results at a qualitative level. If we want to reach quantitative accuracy in our calculations we necessarily have to try with the complete problem, i.e., with the complete evaluation of Eq. (21). We will report about this problem in a future paper.

## X. CONCLUSIONS

The main result of this paper is Eq. (20) in all its variations. This equation is not new in the literature, it has been already written in other reports. However, it is exhaustively studied in the framework of the contraction of the description formalism we developed for depletion interactions. It tells us how to calculate the depletion potential between two particles of a given species immersed in a colloidal suspension where other species are also present. The approximation (21), where the difference between the bridge functions is neglected, results to be very accurate, at least for the case in which the depletion interactions are only of entropic nature. In order of importance we then have Eq. (24) in all its variations. It is obtained from the dilute limit in Eq. (20) and corresponds to the Asakura-Oosawa approximation. Therefore, Eq. (24) is also not new in the literature, but written in a different form given in this paper. We exploited that feature in order to systematically study a large variety of colloidal systems of spherical and nonspherical particles, in two and in three dimensions, in the bulk and in front of a hard wall with a relief pattern. The main proposal in this paper is that the equations for the structure of complex liquids in equilibrium should keep the same form when a contraction of the description is performed. This idea applied to the Ornstein-Zernike equation leads to the results enumerated above.

Although this paper is dedicated to dilute systems, we perform some simulations and theoretical calculations for systems concentrated in the contracted species in order to test the accuracy of our approximations and the correctness of the interpretations we give to our theoretical developments. Moreover, we were able to show that the concentration effects and energetic contributions to the depleting interactions arise from the formation of multiple bridges of contracted particles between two given particles of the observable species.

While studying the depletion interaction between two large spherical particles induced by small spherocylinders we found that the Asakura-Oosawa approximation does not include the effects of the rotational contributions to the entropy, although it is often the belief. Those contributions can be very important, but the correlations between the spherocylinders, which are neglected at the level of AO, must be included in the theory in order to capture them. Anyway, rod-like particles are found to be able to induce larger and more long-ranged depletion attractions than spherical particles with similar parameters.

The inhomogeneous version of Eq. (24) allows us to calculate the depletion interaction between spherical particles and structured hard walls, i.e., hard walls with a relief pattern. Convex regions of the wall are found to interact weakly with the particles, while the concave regions become very attractive. The crossover from a convex to a concave region

is found to induce a depletion force parallel to the wall. Therefore, it may be possible to design walls able to capture the colloidal particles in both directions, perpendicular and parallel to the wall, which could be of technological relevance.

Finally, we would like to point out that our approach works fine in both even and odd dimensions.

## ACKNOWLEDGMENTS

The authors thank PROMEP and CONACyT for financial support (Grants Nos. 33815-E, 0072 “Biomolecular Materials,” 46373/A-1, and 47200/A-1). R.C.P. would like to thank R. Roth for useful discussions.

- 
- [1] S. Asakura and F. Oosawa, *J. Chem. Phys.* **22**, 1255 (1954).  
 [2] A. Vrij, *Pure Appl. Chem.* **48**, 471 (1976).  
 [3] H. N. W. Lekkerkerker and A. Stroobats, *Physica A* **195**, 387 (1993).  
 [4] Y. Mao, M. E. Cates, and H. N. W. Lekkerkerker, *Physica A* **222**, 10 (1995).  
 [5] Y. Rosenfeld, *Phys. Rev. Lett.* **72**, 3831 (1994).  
 [6] R. Roth, R. Evans, and S. Dietrich, *Phys. Rev. E* **62**, 5360 (2000).  
 [7] B. Götzelmann, R. Evans, and S. Dietrich, *Phys. Rev. E* **57**, 6785 (1998).  
 [8] J. M. Méndez-Alcaraz and R. Klein, *Phys. Rev. E* **61**, 4095 (2000).  
 [9] P. B. Warren, S. M. Ilett, and W. C. K. Poon, *Phys. Rev. E* **52**, 5205 (1995).  
 [10] H. H. von Grünberg and R. Klein, *J. Chem. Phys.* **110**, 5421 (1999).  
 [11] P. González-Mozuelos and J. M. Méndez-Alcaraz, *Phys. Rev. E* **63**, 021201 (2001).  
 [12] H. M. Schaink and J. A. M. Smit, *J. Chem. Phys.* **107**, 1004 (1997).  
 [13] Y. Mao, M. E. Cates, and H. N. W. Lekkerkerker, *Phys. Rev. Lett.* **75**, 4548 (1995).  
 [14] Y. Mao, M. E. Cates, and H. N. W. Lekkerkerker, *J. Chem. Phys.* **106**, 3721 (1997).  
 [15] R. Roth, B. Götzelmann, and S. Dietrich, *Phys. Rev. Lett.* **83**, 448 (1999).  
 [16] L. Harnau, F. Penna, and S. Dietrich, *Phys. Rev. E* **70**, 021505 (2004).  
 [17] P. González-Mozuelos, J. M. Méndez-Alcaraz, and R. Castañeda-Priego, *J. Chem. Phys.* **123**, 214907 (2005).  
 [18] R. Castañeda-Priego, A. Rodríguez-López, and J. M. Méndez-Alcaraz, *J. Phys.: Condens. Matter* **15**, S3393 (2003).  
 [19] R. Roth and P. M. König, *Pramana, J. Phys.* **64**, 971 (2005).  
 [20] R. Evans, *Adv. Phys.* **28**, 143 (1979).  
 [21] M. Medina-Noyola and D. A. McQuarrie, *J. Chem. Phys.* **73**, 6279 (1980).  
 [22] P. González-Mozuelos and M. D. Carbajal-Tinoco, *J. Chem. Phys.* **109**, 11074 (1998).  
 [23] J. A. Anta and S. Lago, *J. Chem. Phys.* **116**, 10514 (2002).  
 [24] J. P. Hansen and I. R. McDonald, *Theory of Simple Liquids* (Academic, London, 1986).  
 [25] F. J. Rogers and D. A. Young, *Phys. Rev. A* **30**, 999 (1984).  
 [26] T. Biben and J.-P. Hansen, *Phys. Rev. Lett.* **66**, 2215 (1991).  
 [27] T. Biben and J.-H. Hansen, *J. Phys.: Condens. Matter* **3**, F65 (1991).  
 [28] A. B. Bhatia and D. E. Thornton, *Phys. Rev. B* **2**, 3004 (1970).  
 [29] S. Sanyal, N. Easwar, S. Ramaswamy, and A. K. Sood, *Europhys. Lett.* **18**, 107 (1992).  
 [30] J. S. van Duijneveldt, A. W. Heinen, and H. N. W. Lekkerkerker, *Europhys. Lett.* **21**, 3 (1993).  
 [31] S. M. Ilett, W. C. K. Poon, P. N. Pusey, A. Orrock, M. K. Semmler, and S. Erbit, *Prog. Colloid Polym. Sci.* **97**, 80 (1994).  
 [32] U. Steiner, A. Meller, and J. Stavans, *Phys. Rev. Lett.* **74**, 4750 (1995).  
 [33] A. Imhof and J. K. G. Dhont, *Phys. Rev. Lett.* **75**, 1662 (1995).  
 [34] A. D. Dinsmore, A. G. Yodh, and D. J. Pine, *Phys. Rev. E* **52**, 4045 (1995).  
 [35] M. Dijkstra, R. van Roij, and R. Evans, *Phys. Rev. Lett.* **81**, 2268 (1998).  
 [36] M. Dijkstra, R. Roij, and R. Evans, *Phys. Rev. Lett.* **82**, 117 (1999).  
 [37] M. Dijkstra, R. van Roij, and R. Evans, *Phys. Rev. E* **59**, 5744 (1999).  
 [38] M. López de Haro, private communication.  
 [39] M. P. Allen and D. J. Tildesley, *Computer Simulation of Liquids* (Oxford Science Publications, New York, 1993).  
 [40] T. Biben, P. Bladon, and D. Frenkel, *J. Phys.: Condens. Matter* **8**, 10799 (1996).  
 [41] R. Tehver, A. Maritan, J. Koplik, and J. R. Banavar, *Phys. Rev. E* **59**, R1339 (1999).  
 [42] J. M. Méndez-Alcaraz, B. D’Aguanno, and R. Klein, *Langmuir* **8**, 2913 (1992).  
 [43] K. C. Ng, *J. Chem. Phys.* **61**, 2680 (1974).  
 [44] R. Klein, in *Neutron, X-rays and Light: Scattering Methods Applied to Soft Condensed Matter*, edited by P. Lindner and Th. Zemb (North-Holland, Amsterdam, 2002).  
 [45] F. Lado, *J. Comput. Phys.* **8**, 417 (1971).  
 [46] K. Hiroike, *J. Phys. Soc. Jpn.* **27**, 1415 (1969).  
 [47] P. González-Mozuelos, M. Medina-Noyola, B. D’Aguanno, J. M. Méndez-Alcaraz, and R. Klein, *J. Chem. Phys.* **95**, 2006 (1991).  
 [48] P. González-Mozuelos, J. Alejandro, and M. Medina-Noyola, *J. Chem. Phys.* **95**, 8337 (1991).  
 [49] P. González-Mozuelos, J. Alejandro, and M. Medina-Noyola, *J. Chem. Phys.* **97**, 8712 (1992).  
 [50] P. González-Mozuelos, *J. Chem. Phys.* **98**, 5747 (1993).  
 [51] P. González-Mozuelos and J. Alejandro, *J. Chem. Phys.* **105**, 5949 (1996).  
 [52] S. Fraden and R. D. Kamien, *Biophys. J.* **78**, 2189 (2000).  
 [53] A. D. Dinsmore, A. G. Yodh, and D. J. Pine, *Nature (London)* **383**, 239 (1996).  
 [54] A. D. Dinsmore and A. G. Yodh, *Langmuir* **15**, 314 (1998).  
 [55] K. Yaman, C. Jeppesen, and C. M. Marques, *Europhys. Lett.* **42**, 221 (1998).  
 [56] R. Roth, *J. Phys.: Condens. Matter* **15**, S277 (2003).  
 [57] K. Lin, J. C. Crocker, A. C. Zeri, and A. G. Yodh, *Phys. Rev. Lett.* **87**, 088301 (2001).